Synthesis, Characterization, and Photoluminescence Properties of Boron Tropolonate Complexes: From Fluorescence to Room Temperature Phosphorescence

Hikari Ogoshi,[1] and Shunichiro Ito,[1] and Kazuo Tanaka*[1]

[1]Department of Polymer Chemistry, Graduate School of Engineering, Kyoto University, Katsura, Nishikyo-ku, Kyoto 615-8510, Japan

E-mail: tanaka@poly.synchem.kyoto-u.ac.jp

Kazuo Tanaka

Kazuo Tanaka received his Ph.D. degree in 2004 from Kyoto University, and worked at Stanford University, USA, Kyoto University, and RIKEN as a postdoctoral fellow. In 2007, he moved to the Department of Polymer Chemistry, Graduate School of Engineering, Kyoto University, and in 2018, he was promoted to Professor. His research projects especially focus on design of new functional materials relating optics and nanotechnology based on the heteroatom-containing conjugated polymers and organic-inorganic polymer hybrids.

Abstract

Boron complexes based on tropolone, a seven-membered non-benzenoid aromatic compound, were synthesized. We revealed that the aromaticity of tropolone was enhanced by boron complexation. Importantly, all boron complexes exhibited photoluminescence, and room-temperature phosphorescence (RTP) was observed from the halogenated derivatives, BrTpB and ITpB in the crystalline states. Furthermore, a non-substituted complex, TpB, showed phosphorescence without any heavy atoms in the solution state at 77 K. DFT calculation data suggest that TpB should have large spin-orbit coupling (SOC) constants enough to accept the intersystem crossing. The RTP of halogenated complexes were achieved by heavy atom effects. Significantly, this is the first report of RTP from boron tropolonate complexes.

Keywords: Tropolone, Boron complex, Photoluminescence

1. Introduction

α-Tropolone, or simply tropolone, is a cyclic α-hydroxyketone characterized by the unsaturated seven-membered ring with the 6π-aromatic resonance structure, namely a non-benzenoid aromatic structure. Its peculiar structure was found in natural products, such as hinokitiol,[1,2] stipitatic acid,[3] and colchicine.[4] Since the structure of tropolone itself was determined,[5–8] many studies on the synthesis, characterization, and properties of tropolone derivatives have attracted broad attention.[9] For instance, tropolone derivatives show various biological activities, like antibacterial ability of hinokitiol and colchicine for gout treatment.[10] Besides the research on the biological activities, photophysical and photochemical properties of tropolone derivatives have also been studied.[11,12] Accordingly, it was revealed that the absorption, emission, and photochemical properties of tropolone are highly dependent on solvent and pH. Such sensitivity would be derived from the existence of the acidic proton and the enhanced aromaticity in its anion form.[12] In the studies of colchicine, its photoluminescence has been utilized for evaluating the interactions between colchicine and tubulin.[13] Its fluorescence quantum yield was dramatically enhanced from about 10^{-3} to 0.03 accompanied by binding to tubulin.

Meanwhile, photophysical properties of tropolone-based complexes have also been studied. The tropolonate anion works as a ligand to form chelates with various kinds of metals involving typical elements as well as alkaline earth metals, transition metals, and lanthanides. Historically, Nozoe found out that hinokitin, which is a dark red compound obtained from the residue of taiwanhinoki, was an iron complex of hinokitiol.[1,9] Douglas *et al.* revealed that tropolonate complexes of transition metals are often colored by ligand-to-metal charge-transfer transition.[14] On the other hand, there are few systematic reports on the detailed photophysical properties of typical-element tropolonate complexes.

It is commonly known that tetra-coordinated boron complexes have excellent photophysical properties because of their planar π-conjugated structures, such as boron dipyrromethene (BODIPY) and boron β-diketonates.[15–17] The boron complexation fixes the ligand and results in efficient luminescence quantum yield up to unity. In addition, many types of boron complexes exhibit promising solid-state emission properties involving aggregation-induced and crystallization-induced emission.[18–22] Furthermore, some derivatives of these boron complexes exhibit emission *via* triplet excited states, *i.e.* room-temperature phosphorescence (RTP) [23–25] and thermally activated delayed fluorescence.[26] Hence, these luminophores have been applied to broad fields, for instance, biological imaging,[27] organic light-emitting diodes,[28] and mechanochromic sensors.[29,30] Recently, novel biocompatible fluorophores based on boron complexes of 2-aminotropone scaffolds have been developed.[31] It was demonstrated that the electronic structure has an impact on the luminescence of the complexes. Furthermore, the quantum yields of this class of complexes can be modulated by employing amino acid as the amine moiety and reached up to 16%.[32]

These developments imply that boron complexes based on the tropolone scaffold could give us a novel series of luminescent materials with unique photophysical properties derived from their non-benzenoid aromatic structure. However, the fundamental photoluminescent properties of the boron complexes of tropolone have not been reported, although electronic absorption properties of boron tropolonate was reported.[33] In this study, we synthesized boron complexes based on tropolone and its derivatives to unveil their electronic structures and photophysical properties. Importantly, we found that the halogenated derivatives showed room-temperature phosphorescence in the crystalline states.

2. Experimental

2.1 General experimental details

^{1}H (400 MHz), ^{13}C{^{1}H} (100 MHz), and ^{11}B{^{1}H} (128 MHz) NMR spectra were recorded on JEOL JNM-EX400 or JNM-AL400 spectrometers. ^{1}H NMR spectra were recorded by using tetramethylsilane (TMS) as an internal standard in CDCl$_3$, CD$_2$Cl$_2$, and CD$_3$OD. ^{13}C NMR spectra were recorded by using residual non-deuterated solvents as an internal standard in CDCl$_3$, CD$_2$Cl$_2$, and CD$_3$OD. The ^{11}B chemical shift values were expressed relative to BF$_3$·Et$_2$O as an external standard. High-resolution mass (HRMS) spectrometry was performed at the Technical Support Office (Department of Synthetic Chemistry and Biological Chemistry, Graduate School of Engineering, Kyoto University), and the HRMS spectra were obtained on a Thermo Fisher Scientific EXACTIVE spectrometer for electrospray ionization (ESI) and atmospheric pressure chemical ionization (APCI). UV–vis absorption spectra were recorded on a Shimadzu UV-3600 spectrophotometer. Fluorescence and phosphorescence emission spectra and phosphorescence decay were measured with a HORIBA JOBIN YVON Fluorolog-3 spectrofluorometer and Oxford Optistat DN for temperature control. Absolute photoluminescence quantum yields were measured with a Hamamatsu Photonics Quantaurus-QY Plus C13534-01. Photoluminescence (PL) lifetimes were measured by a Horiba FluoroCube spectrofluorometer system.

2.2 Materials

Commercially available compounds used without purification:

Tropolone (Tokyo Chemical Industry Co, Ltd.; TCI), BF$_3$·OEt$_2$ (Sigma-Aldrich Co. LLC.; Sigma-Aldrich), benzyltrimethylammonium tribromide (TCI), benzyltrimethylammonium dichloroiodate (TCI), calcium carbonate (Wako).

Commercially available solvents:

Dichloromethane (Wako), chloroform (Wako), methanol (Wako), ethanol (Wako), ethylene glycol dimethyl ether (DME) (Wako), and toluene (Wako) were used without further purification. Triethylamine (NEt$_3$) (Kanto Chemical Co., Inc.) was purified using a two-column solid-state purification system (Glasscontour System, Joerg Meyer, Irvine, CA).

3. Results and Discussion

Synthesis of three kinds of boron tropolonate complexes, **TpB**, **BrTpB** and **ITpB**, are shown in Scheme 1. The regioselective bromination of tropolone was carried out according to the literature with benzyltrimethylammonium tribromide.[34] The regioselective iodination was accomplished by employing benzyltrimethylammonium dichloroiodate. Tropolone and its dihalogenated derivatives were subjected to boron complexation by the reaction with boron trifluoride diethyl etherate in the presence of triethylamine. The chemical structures of **TpB**, **BrTpB**, and **ITpB** were confirmed by ^{1}H, ^{13}C{^{1}H}, and ^{11}B{^{1}H} NMR spectroscopy and high-resolution mass spectrometry (HRMS). ^{1}H NMR spectra of **TpB** showed only three characteristic peaks in the low-field region (8.10, 7.87, and 7.73 ppm), indicating the aromatic feature of the seven-membered ring. In the cases of dihalogenated complexes, only two signals were observed in each ^{1}H NMR spectrum. Consequently, the halogenation reactions afforded the regioselectively substituted compounds. The relatively low isolated yields of the boron complexation reactions were mainly due to the loss in purification for obtaining highly pure samples for optical measurements. Thin-layer chromatography indicated the quantitative conversion and no significant side

reactions in the complexation.

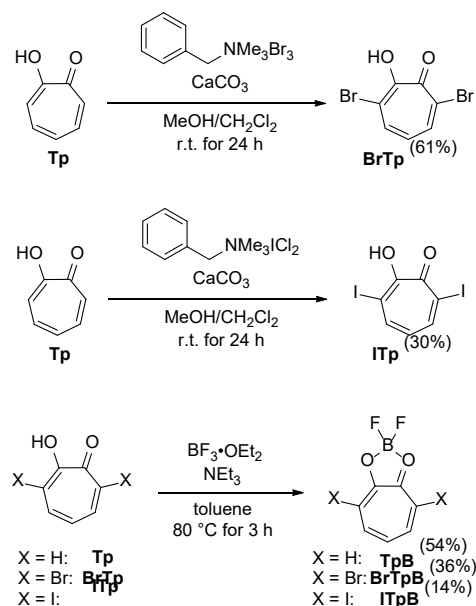**Scheme 1.** Synthesis of boron tropolonate complexes

Figure 1 shows photographic images of the CH$_2$Cl$_2$ solutions and crystalline solids under UV irradiation (375 nm). **TpB** exhibited blue emission both in solution and solid states. To the best of our knowledge, this is the first example of photoluminescence of the simplest boron tropolonate complex, **TpB**. In contrast, the solutions of **BrTpB** and **ITpB** emitted quite weak luminescence, implying the fast non-radiative decay through triplet states. In the crystalline state, **BrTpB** showed orange emission with low intensity. Interestingly, **ITpB** exhibited two distinct states with different emission color and intensity, named as states α (orange emission) and β (red emission). These states were obtained by recrystallization from different solvents: State α was often observed in the recrystallization batches with chloroform, while state β was obtained usually from ethyl acetate. Single crystals corresponding to α and β states were able to be grown. The crystals for α and β states exhibited different crystal habits of prism and needle, respectively (Figure 1).
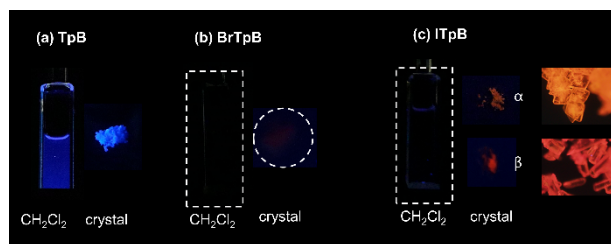

Figure 1. Photographic images of CH$_2$Cl$_2$ solutions (1.0 × 10^{-5} M) and crystalline solids of (a) **TpB**, (b) **BrTpB**, and (c) **ITpB** under UV irradiation (365 nm). Inset: fluorescence microscope images for **ITpB-α** and **ITpB-β**.

Single-crystal X-ray diffraction (SCXRD) analysis revealed that both α and β states of **ITpB** shared the same crystal structure with the slight differences in the lattice parameters (Figure 2g and Table 1). This difference seems to be within a statistical error in the experiment. Indeed, we observed similar extent of differences when other crystals for each state were subjected to the crystal analysis (Table S4). It is well-known that some compounds show dissimilar crystal

habits depending on the solvent due to the difference in solvent–surface interactions.[35] Therefore, we concluded that these two states of **ITpB** had the same crystal structure and were different only in their crystal habits caused by the crystal growth in different crystal faces.

The results of SCXRD for the other complexes were also summarized in Figure 2 and Table 1. All crystals of the complexes belonged to the monoclinic space groups. All atoms except fluorine atoms were coplanar with the carbon atoms of the seven-membered ring. Two molecules were paired up with ca. 3.6 Å of the distance between them so that the static dipole moments were canceled out (Figure 2d–f). Overlapping between the two adjacent seven-membered rings was the largest for **TpB** among the three complexes. Importantly, apparent bond length alternation, which was observed in the parent tropolone structure,[36] was hardly observed in the C1–C7 ring of the boron complexes, although the C1–C2 bond (1.429(2) Å for **TpB**) was slightly longer than the others (1.38–1.39 Å for **TpB**). In addition, the CO bond length (1.323(1) Å for **TpB**) was between the standard CO single and double bonds (1.43 and 1.23 Å, respectively). These facts indicate that each complex has the C_{2v} point group and forms 10π electron systems involving two oxygen and seven carbon atoms, as suggested for sodium tropolonate.[37] These structural features of boron tropolonate derivatives were consistent with the recently reported crystal structure of **TpB**.[38] The harmonic oscillator model of aromaticity (HOMA)[39,40] was employed for comparing the aromaticity before and after the boron complexation. The larger value of HOMA of **TpB** (0.971) than that of tropolone (0.892) suggested the boron complexation enhanced the aromaticity in the seven-membered ring. Anisotropy of the induced current density (ACID) calculations were also performed for the crystal structure of **TpB** as well as tropolone to evaluate their aromaticity.[41,42] The diatropic ring currents were observed in the ACID plots for both **TpB** and tropolone, indicating the delocalization of π-electrons through the C1–C2 bond and their aromaticity in the seven-membered ring (Figure S13). In addition, nucleus-independent chemical shift (NICS) calculations[43] were carried out for the seven-membered ring of **TpB** and tropolone. The NICS(0) and NICS(1) values were calculated as negative values and their absolute values of **TpB** were larger than those of tropolone, suggesting the enhanced aromaticity of **TpB** compared to tropolone (Figure S14).

Table 1. Crystallographic data of synthesized complexes

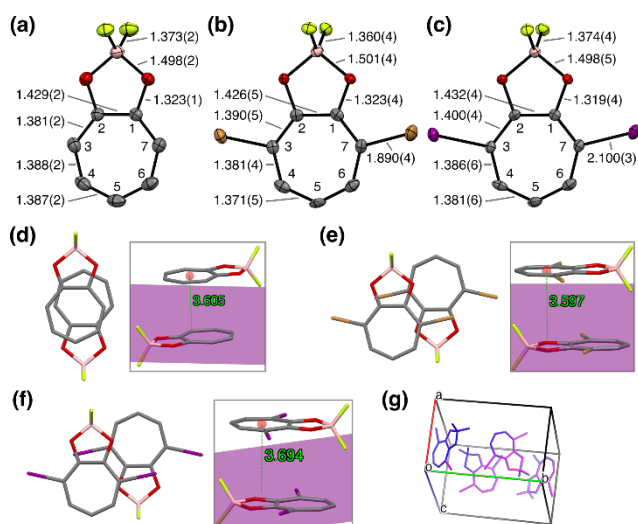|	Space group	a / Å	b / Å	c / Å	β / °	V / Å³
TpB	$P2_1/c$	6.824 (10)	13.560 (18)	7.737(11)	99.72(2)	705.8 (17)
BrTpB	$P2_1/n$	8.083 (5)	13.082 (7)	9.421(7)	116.62 3(9)	890.6 (10)
ITpB -α	$P2_1/c$	8.483 (3)	13.634 (5)	9.223(4)	113.17 5(5)	980.7 (7)
ITpB -β	$P2_1/c$	8.467 (4)	13.611 (6)	9.197(4)	113.11 3(6)	974.8 (7)

Figure 2. ORTEP drawings of (a) **TpB**, (b) **BrTpB**, and (c) **ITpB** (50% probability for thermal elipsoids). Hydrogen atoms are omitted for clarity. Selected bond lengths are shown in Å scale. The number in parentheses represents the standard uncertainty in the last digit. Grey, pink, red, light green, brown, and purple speres represent carbon, boron, oxygen, fluorine, bromine, and iodine, respectively. Dimeric structures in single crystals of (d) **TpB**, (e) **BrTpB**, and (f) **ITpB**. Purple planes and red semitransparent spheres represent the least-square plane and centroid for the seven-membered ring, respectively. Distance between the least-square plane and centroid is shown in Å scale. (g) Superimposed unit cell structures of α (magenta) and β (blue) states of **ITpB**.

To evaluate the electronic structures of each complex without the effect of intermolecular interaction, we measured UV−vis absorption and photoluminescence (PL) spectra of dilute dichloromethane solutions (1.0 × 10⁻⁵ M) as shown in Figure 3, Table 2, and Figure S3. The emission from all the complexes were identified as fluorescence because of their nanosecond-order lifetimes (Figure S4 and Table S). No apparent phosphorescence was observed from these solutions. **TpB** showed the moderate-strength absorption band with the peak at 362 nm, similarly to tropolone in low polarity solvents.[11,12,44] In addition, the photoluminescence quantum yield (Φ_{PL}) of **TpB** (0.04) was significantly higher than the reported value for tropolone (0.005 in cyclohexane).[12] These results imply that the boron complexation could expel non-radiative deactivation paths of tropolone. It is worth noting that any photocyclization reaction of **TpB** was not observed in the spectroscopic measurements, despite the fact that the 4-π-photocyclizations of tropolone derivatives are well-known.[45] Such photostability of **TpB** might be derived from its enhanced aromaticity.

Compared with **TpB**, the absorption and emission bands of **BrTpB** showed the bathochromic shifts probably caused by the extension of electronic conjugation over bromine. The absorption spectrum of **ITpB** also shifted to the lower-energy region than that of **TpB**. On the other hand, for **ITpB**, the strong absorption band in the UV region was split into two or more peaks. In addition, the fluorescence of **ITpB** significantly depended on the excitation wavelengths, while such dependency was not observed from **TpB** and **BrTpB** (Figure S3). When excited at the lowest-energy absorption band (392 nm), the emission peak wavelength was located at 516 nm, which was assigned to the emission from the S_1 state because of the nanosecond-order lifetime. When **ITpB** was excited at 307 nm, its emission band appeared with the peak at 386 nm,

indicating the anti-Kasha emission. In addition, Φ_{PL} values of **BrTpB** and **ITpB** (< 0.01) were smaller than that of **TpB** (0.04), suggesting that the strong heavy atom effect of Br and I should accelerate nonradiative decay of **BrTpB** and **ITpB** through the triplet excited states.
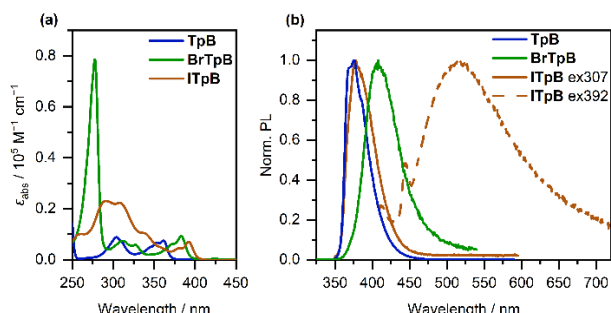

Figure 3. (a) UV–vis absorption and (b) normalized PL spectra of the synthesized complexes in CH_2Cl_2 (1.0×10^{-5} M) at room temperature. Excitation wavelengths: **TpB**, 304 nm; **BrTpB**, 277 nm; **ITpB**, 307 and 392 nm.

Table 2. Photophysical properties of the synthesized complexes in the dilute solutions

	λ_{abs} / nm	ε / 10^4 M^{-1} cm^{-1} ^{a}	λ_{PL} / nm^b	Φ ^{c}
TpB	304, 354, 362	0.89 (362)	374 (304)	0.04
BrTpB	277, 312, 327, 383	7.9 (277)	409 (277)	<0.01
ITpB	292, 308, 381, 392	2.3 (292)	386 (307) 515 (392)	<0.01

^{a}Molar absorption coefficient at the absorption maxima shown in the parentheses. ^{b}Excitation wavelength shown in the parentheses. ^{c}Photoluminescence quantum yield determined with the integrated sphere method.

We also measured PL spectra of 2-methyltetrahydrofuran solutions (1.0×10^{-5} M) at 77 K as shown in Figure 4 and Table 3. These spectra had clearer vibrational structures than those at room temperature because of the restriction of molecular motions. All the complexes showed two distinct emission bands in the steady-state spectra. Time-resolved PL spectra and PL decay measurements (Figures S6–8 and Tables S7) revealed that the emission bands in the shorter- and longer-wavelength regions were assigned to fluorescence and phosphorescence, respectively. The phosphorescence intensity (400–500 nm) of **TpB** was weaker than fluorescence (325–400 nm). Interestingly, there were two components in both fluorescence and phosphorescence of **TpB**. The lower-energy components (359 nm for fluorescence and 515 nm for phosphorescence) could be emission from the lowest excited states, S_1 and T_1, respectively. The higher-energy ones (334 for fluorescence and 405 nm for phosphorescence) would be from the higher excited states, S_n and T_n, respectively. The emission peaks located at 368 and 378 nm for fluorescence are attributed to the vibrational structures of S_1 emission. These results suggest that **TpB** should exhibit anti-Kasha emissions from both singlet and triplet states at 77 K. The S_1/S_n gap (0.26 eV, 2000 cm^{-1}) seemed to be small enough for the S_1 excitons to repopulate to the S_n state, while the T_1/T_n gap (0.67 eV, 5400 cm^{-1}) was large enough to suppress the internal conversion from T_n to T_1.[46] On the other hand, **BrTpB** and **ITpB** showed enhanced phosphorescence properties because of the heavy atom effect of the halogen

substituents. Clear vibrational structures were observed in phosphorescence from the halogenated derivatives. Notably, the remarkably high phosphorescence quantum yields were observed from **BrTpB** (0.44) and **ITpB** (0.59), strongly indicating the efficient heavy atom effect. The higher quantum yield of **ITpB** originated from the efficient intersystem crossing by the stronger heavy atom effect of iodine. It is interesting to note that the relative intensities of the anti-Kasha emission components of **BrTpB** and **ITpB** were quite smaller than those of **TpB** (Figure S6).
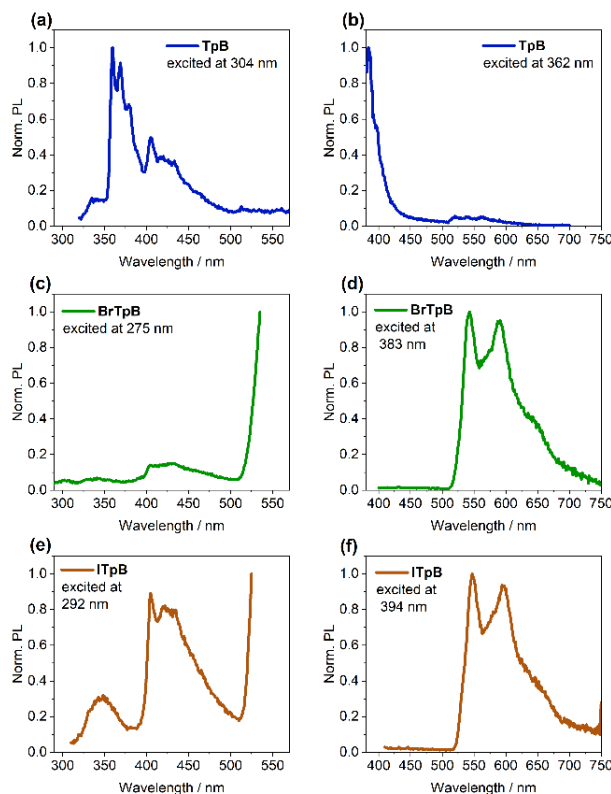

Figure 4. Normalized steady-state PL spectra of the synthesized complexes in 2-methyltetrahydrofuran (1.0×10^{-5} M) at 77 K.

Table 3. Photophysical properties of the synthesized complexes in the dilute solutions at 77 K

	λ_{ex}/ nm^a	λ_{PL} / nm		Φ_{PL}^b	
		Fluo.	Phos.	Fluo.	Phos.
TpB	304	334, 359, 368, 378	405, 515	0.20	0.05
	362	n.d.	520	n.d.	n.d.
BrTpB	275	345, 404, 431	n.d.	<0.01	0.44
	383	n.d.	543, 590	n.d.	n.d.
ITpB	292	350, 404	n.d.	<0.01	0.59
	394	n.d.	547, 594	n.d.	n.d.

^{a}Excitation wavelength. ^{b}Absolute photoluminescence quantum yield determined with the integrated sphere method. Excitation wavelengths: **TpB**, 304 nm; **BrTpB**, 278 nm; **ITpB**, 292 nm. (n.d.: Not determined.)

The optical properties of the synthesized complexes in crystalline states were evaluated (Figure 5 and Table 4). Powder X-ray diffraction patterns of the solid samples used for the photophysical measurements agreed with the estimated profiles from the SCXRD results (Figure S2), indicating that the solid-state structures of these samples were identical to those of the single crystals. **TpB** exhibited only sharp

fluorescence at 386 nm, which was similar to the behavior in its solution. The fluorescence band of **TpB** in the solid state was broader than in the solution state probably due to the intermolecular interactions. Meanwhile, both **BrTpB** and **ITpB** showed RTP in the region of 550–700 nm. Most importantly, the heavy atom effect of bromine and iodine facilitated the detectable RTP from the crystals, although the overall quantum yields were smaller than the limit of quantitative measurement. **BrTpB** emits fluorescence at 414 nm in addition to the phosphorescence, indicating that the radiative decay from the singlet excited state competed with the intersystem crossing to the triplet excited states. **ITpB**, on the other hand, did not show fluorescence probably because almost all singlet excited states transformed to triplet ones by the rapid intersystem crossing. The optical properties of **ITpB** were different between states α and β, as shown in Figure 5c. Both states exhibited phosphorescence in the similar region (500–750 nm), yet the emission band of state β was relatively broad and structureless. The phosphorescence spectrum of state α was characterized by the significant contribution of the peak at the 542 nm, which was slightly observed in the spectra of state β as a shoulder peak. These results imply that there are at least two distinct luminescent species in the crystal, and their relative intensity could depend on the crystal habit.

To gather further information about the luminescent species of these complexes in the crystalline states, we measured emission decay curves and time-resolved emission spectra (TRES). Interestingly, TRES of **BrTpB** revealed that there were two components in the phosphorescence bands (Figure S9). The shorter-wavelength component (500–600 nm) possessed a shorter lifetime (75 μs) than the longer-wavelength one (600–750 nm, 1.6 ms). The higher-energy and short-lifetime component (500–600 nm) was observed in the similar region of the phosphorescence band in the frozen solution (Figure 4d), implying that this band might be assignable to the emission from single molecules without intermolecular interactions. In contrast, the lower-energy and longer-lifetime emission band (600–750 nm) might be attributed to the lower-energy exciton resulted from intermolecular interactions.

TRES of **ITpB** in crystalline states was also evaluated (Figure S10). Both states α and β had three phosphorescence decay components. The emission band in 500–570 nm was found from both states and attributed to single molecules because this band was also detected in the frozen state as shown in Figure 4f. The other emission species observed in the longer-wavelength region should be derived from intermolecular interactions. The relative phosphorescence intensities of these emission species seemed to be different from state α to state β. As mentioned above, both states share the same crystal structure and are different only in the crystal habits. The differences in the PL spectra and TRES between these states might be caused by the emission from different crystal habits.[47,48]
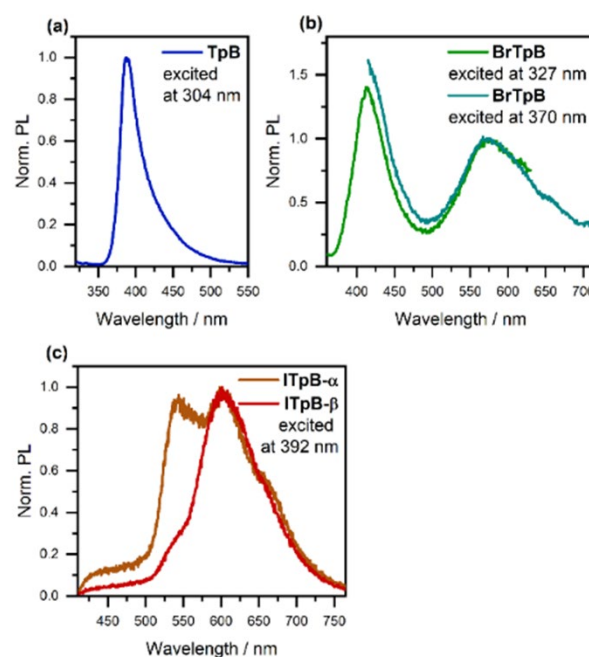

Figure 5. Normalized steady-state photoluminescence spectra of (a) **TpB**, (b) **BrTpB**, and (c) **ITpB** in crystalline states.

Table 4. Photophysical properties of the synthesized complexes in crystalline state[a]

	λ_{PL} / nm		Φ	
	Fluorescence	Phosphorescence	Fluorescence	Phosphorescence
TpB	386	n.d.	0.04	n.d.
BrTpB	414	570, 650	<0.01	<0.01
ITpB-α	n.d.	542, 603	n.d.	<0.01
ITpB-β	n.d.	605	n.d.	0.01

[a]n.d.: Not determined.

In order to explain the series of results, we performed density functional theory (DFT) and time-dependent DFT (TD-DFT) calculations for each complex with the B3LYP functional, the LANL2DZ basis set for iodine and 6-31G(d, p) for the other elements using the Gaussian 16 program package.[49] All the optimized structures were confirmed as each local minimum by using frequency calculations at the same level of theory. Excited state energies for each structure were calculated by Q-Chem 6.0.0. package,[50] TD-DFT and the Tamm–Dancoff approximation.

As shown in Figure 6, the calculated S_0–S_1 transition energies decreased in the order of **TpB** > **BrTpB** > **ITpB**, which agreed with the peak positions of their lowest-energy absorption and S_1–S_0 emission spectra. In addition, the calculations reproduced the experimental order of T_1–S_0 phosphorescence energy (**TpB** > **BrTpB** ~ **ITpB**). Importantly, the S_3 and T_3 states of **TpB** were located significantly far from the S_2 and T_2 states, respectively (energy gap: S_2/S_3, 1.14 eV; T_2/T_3, 1.16 eV). Such large energy gaps between the higher and lower excited states could be responsible for the anti-Kasha fluorescence and phosphorescence of **TpB** observed at 77 K. In addition, the moderate oscillator strength for the S_0–S_3 transition (0.0950) was comparable to that of the S_0–S_1 one (0.1088) and could allow the emission from the S_3 state.

As mentioned above, the anti-Kasha phosphorescence band (405 nm) of **TpB** was hardly observed under the

excitation to the S_1 state rather than the higher S_n states, implying that the higher-energy state should be required for the intersystem crossing for the anti-Kasha phosphorescence. The possibility of intersystem crossing between each singlet and triplet states was evaluated by spin-orbit coupling constants (ξ) calculated with the Q-Chem 6.0.0 package (Tables S14–S16).[50] Even though heavy atoms are not introduced in **TpB**, ξ values are larger than 4 cm^{-1}. These values are large enough to accept intersystem crossing and phosphorescence in the frozen solution state.[53] In particular, non-bonding orbitals corresponding to the lone pairs of the oxygen atoms are found in HOMO–2 and HOMO–4 (Figure 7), which compose the T_5 state of **TpB** (HOMO–2→LUMO and HOMO–4→LUMO+1). The S_1 state, on the other hand, is assigned to the HOMO to LUMO (π–π*) transition. Therefore, the S_1–T_5 transition involves the change in orbital angular momentum, resulting in the enhanced intersystem crossing according to the El-Sayed rule.[54] In addition, the calculated ξ values for **BrTpB** got larger by introducing halogens, reflecting the strong heavy atom effect. The similar heavy atom effect of iodine should be responsible for the RTP from the **ITpB** crystals. The unexpectedly small ξ values calculated for **ITpB** (Table S16) would originate from the node-less inner orbitals of the effective core potential for iodine. Larger values may be obtained by employing other methods such as model core potential or all-electron basis set.[51,52]

Proposed Jablonski diagrams of the complexes are summarized in Figure 8. T_1* and T_n* in **BrTpB** and **ITpB** denote the newly generated triplet states by intermolecular interactions in crystalline states, which showed longer lifetimes as mentioned above. **TpB** showed only fluorescence in both solution and crystalline states at room temperature. It exhibited phosphorescence addition to fluorescence in frozen solution state at 77 K, especially anti-Kasha emission from the higher triplet excited state. **BrTpB** showed both fluorescence and phosphorescence in crystalline state at room temperature. **ITpB** crystal showed phosphorescence in both α and β states. Enhanced phosphorescence was observed in **BrTpB** and **ITpB** in solution states at 77 K. These great phosphorescence properties of halogenated derivatives are caused by strong heavy atom effects of bromine and iodine, respectively. Furthermore, the additional luminescent species for **BrTpB** and **ITpB** could be generated by intermolecular interactions in the crystalline states and responsible for their multi-component RTP.
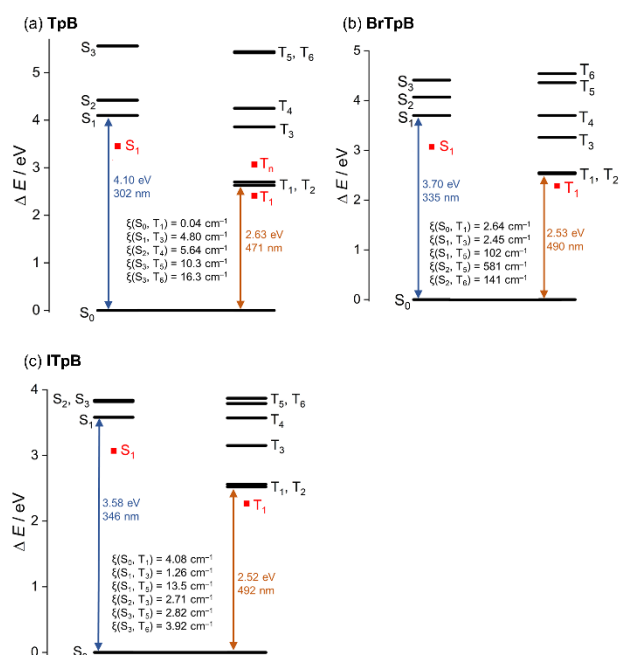

Figure 6. Energy diagrams and spin-orbit coupling coefficients (ξ) of synthesized complexes. Black lines represent the calculated values. S_n and T_n denote n-th singlet and triplet excited states, respectively.
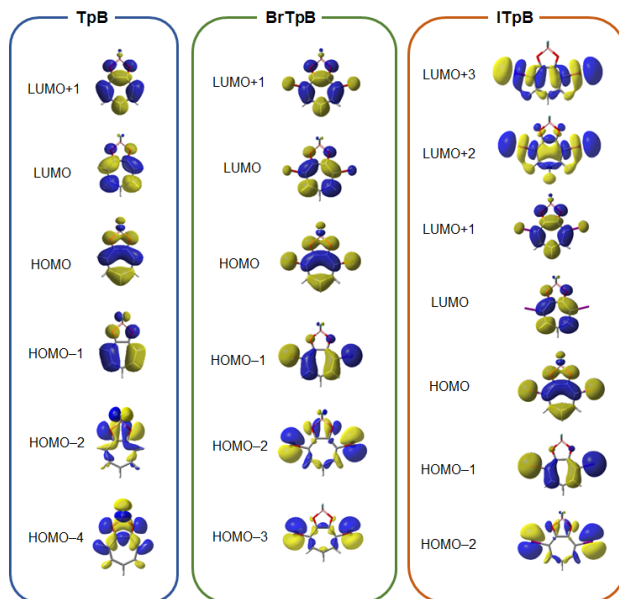

Figure 7. Molecular orbitals of synthesized complexes.
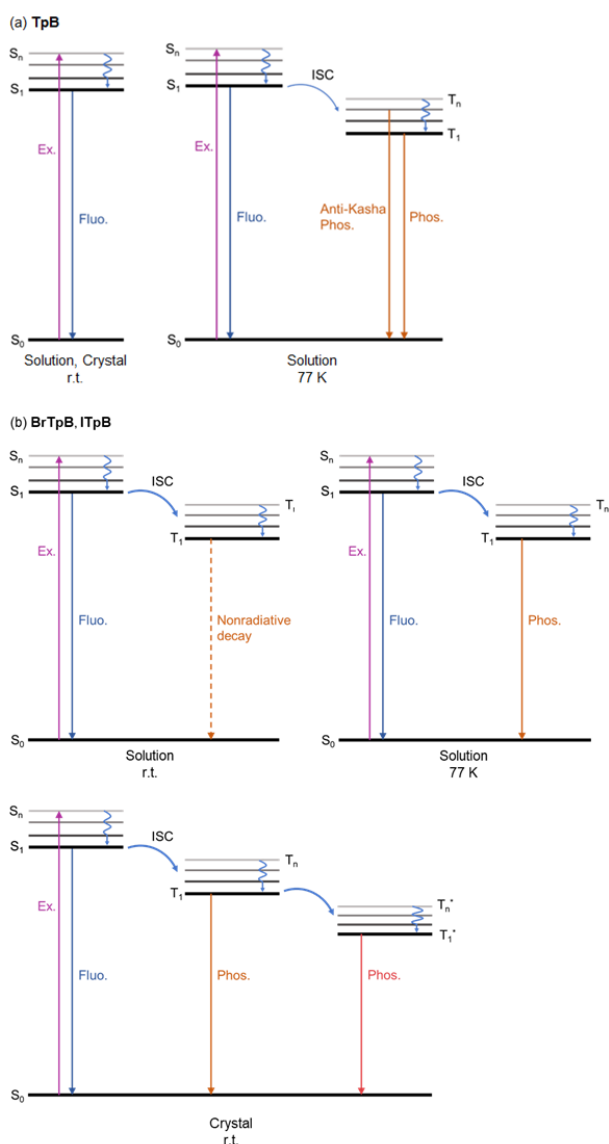
Figure 8. Proposed Jablonski diagrams for (a) **TpB** and for (b) **BrTpB** and **ITpB**. T_1^* and T_n^* in (b) denote the newly generated triplet states by intermolecular interactions in crystalline states.

4. Conclusion

Four-coordinated difluoroboron tropolonate and its halogenated derivatives were synthesized and fully characterized. Structural and theoretical analyses suggest that the boron complexation should enhance the aromaticity of the seven-membered ring. The unsubstituted tropolonate complex **TpB** showed more efficient emission than tropolone itself at room temperature in the solution. Phosphorescence of **TpB** in the frozen solution state was also detected even in the absence of heavy atoms. In addition, it exhibited anti-Kasha phosphorescence from the higher triplet excited state in frozen state due to a large energy gap between triplet excites states. **BrTpB** and **ITpB** showed enhanced phosphorescence emission by the heavy atom effects of bromine and iodine, respectively, in solution states at 77 K. Importantly, these two complexes showed RTP in crystalline states. Interestingly, **ITpB** crystallized into two distinct states, α and β, with different optical properties. SCXRD measurements revealed that these states of **ITpB** shared the same unit cell. Consequently, these different emission behaviors stemmed from the difference in the crystal habits. Additionally, to the best of our knowledge, this is the first report of RTP of tropolone based compounds.

References

1. T. Nozoe, *Bull. Chem. Soc. Jpn.* **1936**, *11*, 295–298.
2. T. Nozoe, *Yakugaku Zasshi*, **1944**, *64*, 181–185 (Japanese).
3. M. J. S. Dewar, *Nature* **1945**, *155*, 50–51.
4. M. J. S. Dewar, *Nature* **1945**, *155*, 141–142.
5. J. W. Cook, A. R. Gibb, R. A. Raphael, A. R. Somerville, *Chem. Ind. (Lond.)* **1950**, *15*, 427.
6. R. D. Haworth, *Chem. Ind. (Lond.)* **1950**, *15*, 441.
7. T. Nozoe, S. Seto, Y. Kitahara, M. Kunori, Y. Nakayama, *Proc. Jpn. Acad.* **1950**, *26*, 38–42.
8. W. von E. Doering, L. H. Knox, *J Am Chem Soc* **1951**, *73*, 828–838.
9. I. Murata, S. Ito, T. Asao, *Eur. J. Org. Chem.* **2004**, *4*, 899–928.
10. N. Liu, W. Song, C. M. Schienebeck, M. Zhang, W. Tang, *Tetrahedron*, **2014**, *70*, 9281–9305.
11. H. Hosoya, J. Tanaka, S. Nagakura, *Tetrahedron* **1962**, *18*, 859–874.
12. E. F. Breheret, M. M. Martin, *J Lumin* **1978**, *17*, 49–60.
13. S. B. Hastie, *Pharmacol. Ther.* **1991**, *51*, 377–401.
14. Y. Dutt, R. P. Singh, M. Katyal, *Talattta.* **1969**, *16*, 1369–1382.
15. D. Li, H. Zhang, Y. Wang, *Chem Soc Rev* **2013**, *42*, 8416–8433.
16. D. Frath, J. Massue, G. Ulrich, R. Ziessel, *Angew. Chem. Int.* **2014**, *53*, 2290–2310.
17. A. C. Murali, P. Nayak, K. Venkatasubbaiah, *Dalton Trans.* **2022**, *51*, 5751–5771.
18. K. Tanaka, M. Gon, S. Ito, J. Ochi, Y. Chujo, *Coord Chem Rev.* **2022**, *472*, 214779.
19. P. Galer, R. C. Korošec, M. Vidmar, B. Šket, *J Am Chem Soc* **2014**, *136*, 7383–7394.
20. R. Yoshii, A. Nagai, K. Tanaka, Y. Chujo, *Chem. Eur. J.* **2013**, *19*, 4506–4512.
21. R. Yoshii, A. Hirose, K. Tanaka, Y. Chujo, *Chem. Eur. J.* **2014**, *20*, 8320–8324.
22. R. Yoshii, A. Hirose, K. Tanaka, Y. Chujo, *J Am Chem Soc* **2014**, *136*, 18131–18139.
23. T. Liu, G. Zhang, R. E. Evans, C. O. Trindle, Z. Altun, C. A. DeRosa, F. Wang, M. Zhuang, C. L. Fraser, *Chem. Eur. J.* **2018**, *24*, 1859–1869.
24. A. Sakai, E. Ohta, Y. Matsui, S. Tsuzuki, H. Ikeda, *ChemPhysChem* **2016**, *17*, 4033–4036.
25. M. Koch, K. Perumal, O. Blacque, J. A. Garg, R. Saiganesh, S. Kabilan, K. K. Balasubramanian, K. Venkatesan, *Angew. Chem. Int. Ed.* **2014**, *53*, 6378–6382.
26. Y. Shiu, Y. Cheng, W. Tsai, C. Wu, C. Chao, C. Lu, Y. Chi,

Y. Chen, S. Liu, P. Chou, *Angew. Chem. Int.* **2016**, *55*, 3017–3021.

27. K. Li, X. Duan, Z. Jiang, D. Ding, Y. Chen, G. Zhang, Z. Liu, *Nat. Commun.* **2021**, *12*, 2376–2386.

28. Y. H. Jung, D. Karthik, H. Lee, J. H. Maeng, K. J. Y, S. Hwang, J. H. Kwon, *ACS Appl. Mater. Interfaces* **2021**, *13*, 17882–17891.

29. G. Zhang, J. Lu, M. Sabat, C. L. Fraser, *J. Am. Chem. Soc.* **2010**, *132*, 2160–2162.

30. J. Song, L. Ma, S. Sun, H. Tian, X. Ma, *Angew. Chem. Int. Ed.,* **2022**, *61*, e202206157.

31. C. Balachandra, N. K. Sharma, *Dyes and Pigments*, **2017**, *137*, 532–538.

32. B. B. Palai, R. Soren, N. K. Sharma, *Org. Biomol. Chem.*, **2019**, *17*, 6497–6505.

33. Brown, N. M. D.; Bladon, P. *J. Chem. Soc. A. Inorg. phys. theor* **1969**, 526–532.

34. S. R. Piettre, A. Ganzhorn, J. Hoflack, K. Islam, J. Hornsperger, *J. Am. Chem. Soc.* **1997**, *119*, 3201–3204.

35. M. Lahav, L. Leiserowitz, *Chem. Eng. Sci.* **2001**, *56*, 2245-2253.

36. H. Shimanouchi, Y. Sasada, *Acta. Crystallogr. B. Struct. Sci. Cryst.* **1973**, *29*, 81–90.

37. Y. Sasada, I. Nitta, *Acta Cryst.* **1956**, *9*, 205–214.

38. A. Budanow, M. Bolte, M. Wagner CCDC 2159284: *Experimental Crystal Structure Determination*, **2022**,

39. J. Kruszewski, T. M. Krygowski, *Tetrahedron Lett* **1972**, *13*, 3839–3842.

40. T. M. Krygowski, H. Szatylowicz, O. A. Stasyuk, J. Dominikowska, M. Palusiak, *Chem. Rev.* **2014**, *114*, 6383–6422.

41. R. Herges, D. Geuenich, *J. Phys. Chem.* **2001**, *105*, 3214–3220.

42. D. Geuenich, K. Hess, F. Köhler, R. Herges, *Chem. Rev.* **2005**, *105*, 3758–3772.

43. Z. Chen, C. S. Wannere, C. Corminboeuf, R. Puchta, P. von R. Schleyer, *Chem. Rev.* **2005**, *105*, 3842–3888.

44. W von E. Doering, L. H. Knox, *J. Am. Chem. Soc.* **1951**, *73*, 828–838.

45. S. C. Coote, *Eur. J. Org. Chem.* **2020**, *2020*, 1405–1423.

46. T. Itoh, *Chem. Rev.* **2012**, *112*, 4541–4568.

47. C. Spies, A. Huynh, V. Huch, G. Jung, *J. Phys. Chem. C* **2013**, *117*, 18163–18169.

48. J. Percino, M. Cerón, P. Venkatesan, P. Ceballos, A. Bañuelos, O. Rodríguez, M. A. Siegler, F. Robles, V. M. Chapela, G. Soriano-Moro, E. Pérez-Gutiérrez, J. Bonilla-Cruz, S. Thamotharan, *Cryst. Growth Des.* **2017**, *17,* 1679–1694.

49. M. J. Frisch, G. W. Trucks, H. B. Schlegel, G. E. Scuseria, M. A. Robb, J. R. Cheeseman, G. Scalmani, V. Barone, G. A. Petersson, H. Nakatsuji, X. Li, M. Caricato, A. V. Marenich, J. Bloino, B. G. Janesko, R. Gomperts, B. Mennucci, H. P. Hratchian, J. V. Ortiz, A. F. Izmaylov, J. L. Sonnenberg, D. Williams-Young, F. Ding, F. Lipparini, F. Egidi, J. Goings, B. Peng, A. Petrone, T. Henderson, D. Ranasinghe, V. G. Zakrzewski, J. Gao, N. Rega, G. Zheng, W. Liang, M. Hada, M. Ehara, K. Toyota, R. Fukuda, J. Hasegawa, M. Ishida, T. Nakajima, Y. Honda, O. Kitao, H. Nakai, T. Vreven, K. Throssell, J. A. Montgomery, Jr., J. E. Peralta, F. Ogliaro, M. J. Bearpark, J. J. Heyd, E. N. Brothers, K. N. Kudin, V. N. Staroverov, T. A. Keith, R. Kobayashi, J. Normand, K. Raghavachari, A. P. Rendell, J. C. Burant, S. S. Iyengar, J. Tomasi, M. Cossi, J. M. Millam, M. Klene, C. Adamo, R. Cammi, J. W. Ochterski, R. L. Martin, K. Morokuma, O. Farkas, J. B. Foresman, and D. J. Fox, Gaussian 16 Rev. C.01, Wallingford, CT, **2016**.

50. E. Epifanovsky, A. T. B. Gilbert, X. Feng, J. Lee, Y. Mao, N. Mardirossian, P. Pokhilko, A. F. White, M. P. Coons, A. L. Dempwolff, Z. Gan, D. Hait, P. R. Horn, L. D. Jacobson, I. Kaliman, J. Kussmann, A. W. Lange, K. U. Lao, D. S. Levine, J. Liu, S. C. McKenzie, A. F. Morrison, K. D. Nanda, F. Plasser, D. R. Rehn, M.L. Vidal, Z. You, Y. Zhu, B. Alam, B. J. Albrecht, A. Aldossary, E. Alguire, J. H. Andersen, V. Athavale, D. Barton, K. Begam, A. Behn, N. Bellonzi, Y. A. Bernard, E. J. Berquist, H. G. A. Burton, A. Carreras, K. Carter-Fenk, R. Chakraborty, A. D. Chien, K. D. Closser, V. Cofer-Shabica, S. Dasgupta, M. de Wergifosse, J. Deng, M. Diedenhofen, H. Do, S. Ehlert, P. Fang, S. Fatehi, Q. Feng, T. Friedhoff, J. Gayvert, Q. Ge, G. Gidofalvi, M. Goldey, J. Gomes, C. E. González-Espinoza, S. Gulania, A. O. Gunina, M. W. D. Hanson-Heine, P. H. P. Harbach, A. Hauser, M. F. Herbst, M. Hernández Vera, M. Hodecker, Z. C. Holden, S. Houck, X. Huang, K. Hui, B. C. Huynh, M. Ivanov, Á. Jász, H. Ji, H. Jiang, B. Kaduk, S. Kähler, K. Khistyaev, J. Kim, G. Kis, P. Klunzinger, Z. Koczor-Benda, J. Hoon Koh, D. Kosenkov, L. Koulias, T. Kowalczyk, C. M. Krauter, K. Kue, A. Kunitsa, T. Kus, I. Ladjánszki, A. Landau, K. V. Lawler, D. Lefrancois, S. Lehtola, R. R. Li, Y. Li, J. Liang, M. Liebenthal, H. Lin, Y. Lin, F. Liu, K. Liu, M. Loipersberger, A. Luenser, A. Manjanath, P. Manohar, E. Mansoor, S. F. Manzer, S. Mao, A. V. Marenich, T. Markovich, S. Mason, S. A. Maurer, P. F. McLaughlin, M. F. S. J. Menger, J. Mewes, S. A. Mewes, P. Morgante, J. W. Mullinax, K. J. Oosterbaan, G. Paran, A. C. Paul, S. K. Paul, F. Pavoševi ć, Z. Pei, S. Prager, E. I. Proynov, Á. Rák, E. Ramos-Cordoba, B. Rana, A. E. Rask, A. Rettig, R. M. Richard, F. Rob, E. Rossomme, T. Scheele, M. Scheurer, M. Schneider, N. Sergueev, S. M. Sharada, W. Skomorowski, D. W. Small, C. J. Stein, Y. Su, E. J. Sundstrom, Z. Tao, J. Thirman, G. J. Tornai, T. Tsuchimochi, N. M. Tubman, S. Prasad Veccham, O. Vydrov, J. Wenzel, J. Witte, A. Yamada, K. Yao, S. Yeganeh, S. R. Yost, A. Zech, I. Y. Zhang, X. Zhang, Y. Zhang, D. Zuev, A. Aspuru-Guzik, A. T. Bell, Software for the frontiers of quantum chemistry:An overview of developments in the Q-Chem 5 package *J. Chem. Phys.* **2021**, *155*, 084801.

51. S. Koseki, N. Matsunaga, T. Asada, M. W. Schmidt, M. S. Gordon, *J. Phys. Chem. A* **2019**, *123*, 2325–2339.

52. D. G. Fedorov, M. Klobukowski, *Chem. Phys. Lett.* **2002**, *360*, 223–228.

53. S. Ji, J. Ge, D. Escudero, Z. Wang, J. Zhao, D. Jacquemin, *J. Org. Chem.* **2015**, *80*, 5958–5963.

54. C. M. Marian, *Wiley Interdiscip. Rev. Comput. Mol. Sci.* **2012**, *2*, 187–203.

Graphical Abstract

<Title>

Synthesis, Characterization, and Photoluminescence Properties of Boron Tropolonate Complexes: From Fluorescence to Room Temperature Phosphorescence

<Authors' names>
Hikari OGOSHI, Shunichiro ITO, Kazuo TANAKA

<Summary>
Boron complexes based on tropolone, a seven-membered non-benzenoid aromatic compound, were synthesized. The aromaticity of tropolone was enhanced by boron complexation. Importantly, all boron complexes exhibited photoluminescence, and room-temperature phosphorescence (RTP) was observed from the halogenated derivatives in the crystalline states. The RTP of halogenated complexes were achieved by heavy atom effects.

<Diagram>